Bakhtiari, S.; Elmer, T. W.; Cox, N. M.; Gopalsami, N.; Raptis, A. C.; Liao, S.; Mikhelson, I.; Sahakian, A. V.; , "Compact Millimeter-Wave Sensor for Remote Monitoring of Vital Signs," Instrumentation and Measurement, IEEE Transactions on , vol.61, no.3, pp.830-841, March 2012

DOI: 10.1109/TIM.2011.2171589

Compact Millimeter Wave Sensor for Remote Monitoring of Vital Signs

Sasan Bakhtiari*, *Senior Member, IEEE*, Thomas W. Elmer, *Member, IEEE*, Nicholas M. Cox, Nachappa Gopalsami, *Senior Member, IEEE*, Appostolos C. Raptis, *Senior Member, IEEE*, Shaolin Liao, *Member, IEEE*
Nuclear Engineering Division, Argonne National Laboratory, 9700. S. Cass Ave., Lemont, IL 60439

Ilya Mikhelson, *Student Member, IEEE,* and Alan V. Sahakian, *Fellow, IEEE*
Electrical and Computer Science Department, Northwestern University, 2145 Sheridan Rd., Evanston, IL 60208

Abstract—A compact millimeter wave (MMW) sensor has been developed for remote monitoring of human vital signs (heart and respiration rate). The low-power homodyne transceiver operating at 94 GHz was assembled by using solid-state active and passive block-type components and can be battery operated. A description of the MMW system front-end and the back-end acquisition hardware and software is presented. Representative test case results on the application of various signal processing and data analysis algorithms developed to extract faint physiological signals of interest in presence of strong background interference are provided. Although the laboratory experiments so far have been limited to standoff distances of up to fifteen meters, the upper limit of the detection range is expected to be higher. In comparison to its microwave counterparts, the MMW system described here provides higher directivity, increased sensitivity, and longer detection range for measuring subtle mechanical displacements associated with heart and respiration functions. The system may be adapted for use in a wide range of standoff sensing applications including for patient health care, structural health monitoring, nondestructive testing, biometric sensing, and remote vibrometry in general.

***Index Terms*—**Millimeter wave sensor, biomedical monitoring, vital signs, remote sensing, signal processing.

I. INTRODUCTION

Remote measurement of physiological signals is the most desirable non-invasive sensing scenario in a number of applications; in healthcare, for in- and out-of-hospital monitoring of patients, in first responder operations, for locating of subjects buried under rubble, and in national and homeland security, for standoff biometric screening. The ability of microwave energy to penetrate through many optically opaque dielectric materials such as common fabrics with relatively low levels of attenuation and reflect strongly from the underlying biological matter renders this electromagnetic frequency range particularly

*Corresponding Author—phone.: 630-252-8982; fax: 630-252-3250; e-mail: bakhtiari@anl.gov

suited for non-invasive probing of physiological movements. The use of microwave techniques for remote monitoring of human vital signs has been investigated by a number of researchers in the past. The majority of work in this area has been conducted within the microwave band—commonly designated as the frequency range between 300 MHz and 30 GHz [1]-[10]. The majority of devices developed for this purpose operate at the lower end of the microwave range in part because of the availability and maturity of the technology in that frequency range, and in part because of the more straight-forward signal processing involved in extracting the displacement information. As a direct result of operating at shorter wavelengths, millimeter-wave (MMW) frequencies—commonly designated as the frequency range between 30 GHz and 300 GHz—provide higher sensitivity than their microwave counterparts for detection of physiological movements. Notably fewer studies, however, have been reported on the use of mid-range MMW technology for remote measurement of human vital signs. Investigations conducted at the upper end of the MMW range on the other hand have employed quasi-optical techniques using table-top systems composed of high-frequency solid-state components and laboratory instruments [11], [12].

The upper range of detection with microwave systems developed for non-contact monitoring of vital signs is typically limited to standoff distances of a few meters. In all the reported cases, the measurements were made with the subject at rest and normally in a seated position. As a direct consequence of operating at centimeter wavelengths, such systems generally suffer from lack of sensitivity (low S/N) to physiological movements in the order of tens of micrometers. At longer standoff distances, interference from unwanted reflections within the antenna beam (e.g., movement of extremities) can significantly limit the ability to isolate faint signals of interest. Highly directional antennas needed for spot focusing and tracking become impractical for vital sign monitoring applications at longer target ranges (tens of meters). Development of systems operating at the upper end of the MMW band, on the other hand, brings about a different set of challenges that include unavailability of off-the-shelf solid-state components. Manufacturing of reliable low-noise amplifiers and quadrature mixers above 150 GHz remains to be an engineering challenge. While feasibility studies on remote monitoring of vital signs have been conducted under laboratory settings, viability of a practical system operating at the upper end of the MMW band has not yet been demonstrated. As discussed later in this paper, MMW frequencies in the W-band range (75-110 GHz) provide a good tradeoff between range and sensitivity for the detection of biosignals of interest. For monitoring applications at standoff distances of tens of meters, Gunn and IMAPTT diode sources are readily available in the W-band with power outputs of up 20 dBm. Operating in the wavelength range of 2.7 mm to 4 mm, W-band phase detectors allow resolving of out-of-plane displacements in the range of a few micrometers. These attributes render the W-band particularly suitable for integration of compact sensors for remote monitoring of vital signs.

The results of investigations in connection with development and testing of a compact MMW sensor operating at 94 GHz for remote monitoring of human vital signs (cardiac and respiration rate) are presented in this article. The research was conducted in part to help close the technology gap in remote monitoring of human vital signs at relatively long standoff distances. In addition to the sensor hardware, a number of signal processing and data analysis routines have also been developed to better detect faint biosignals associated with subtle movements in presence of strong stationary and systematic reflections. The results of experimental investigations carried out to date are presented here.

II. APPROACH

Active and passive MMW radar and radiometry techniques have been employed in the past for various environmental remote sensing applications [13]-[15]. As a direct consequence of operating at shorter wavelengths in comparison with microwave frequencies, MMW technology allows fabrication of more compact devices with superior sensitivity and with higher directivity, obtainable with high-gain aperture antennas of practical size.

A MMW sensor operating at 94 GHz has been developed for remote monitoring of human vital signs at relatively long distances (tens of meters). Past investigations by the authors have demonstrated the ability to resolve micrometer scale displacements at this frequency range, which is at least an order of magnitude smaller than the levels of displacement associated with the chest movements due to heart and respiration functions [16]. The selected waveguide band (WR-10) is within the MMW atmospheric transmission window, thus providing low propagation losses over distances of interest for monitoring of subtle physiological movements. Finally, this waveguide band is currently considered as the upper limit of frequency at which MMW mixers and low-noise amplifiers can be manufactured without facing major engineering challenges.

The basic concept of remote sensing of vibration or displacement is to measure the modulation induced on a coherent signal reflected off of a moving object's surface. Analogous to heterodyne detection of interferometric signals, mixing of the backscattered electromagnetic signal with a portion of the reference transmitted signal (i.e., local oscillator) allows recovery of low-frequency modulations induced by a vibrating target. Line-of-sight displacements may be sensed by either directly measuring the phase modulation, φ, induced by the target on the backscattered carrier signal or by measuring the Doppler frequency shift, f_d. In their basic form, these effects may be expressed as

$$\varphi(t) = \frac{4\pi}{\lambda} d(t) = \frac{4\pi}{\lambda}\left[d_0 + \cos(\theta)\int v(t)dt\right] \tag{1}$$

and

$$f_d(t) = \frac{1}{2\pi}\frac{d\varphi(t)}{dt} = \frac{2v(t)}{\lambda}\cos(\theta) \tag{2}$$

in which λ is the carrier wavelength, $v(t)$ is the velocity of the target, θ is the angle between the direction of target motion and the beam, d_0 is the nominal distance to the target, and $d(t)$ is the displacement. In reference to (1), phase interference of coherent MMW radiation acquired over a period of time may be used to remotely obtain information about the displacement and in turn the vibration frequency of the object.

III. MMW System Configuration

A homodyne MMW interferometer has been developed for remote measurement of physiological displacements. The device was assembled by using solid-state active and passive MMW block-type components. The sensor dimensions (length, width, and depth), excluding the lens antenna, are approximately 7.5x6.5x2.5 cm^3. In reference to Fig. 1, the system front-end employs a W-band (94 GHz) Gunn diode oscillator (GDO) with a nominal output power of 15 dBm and uses a 5 v modulator-regulator as its power supply, which allows for frequency or amplitude modulation of the source. The transmitter was fitted with a heater unit for better frequency stability. The MMW transceiver has a homodyne configuration and directly down-converts the carrier signal by incorporating a W-band quadrature IF mixer—commonly referred to as I-Q mixer. The local oscillator output is split between the reference and the transmitted arm via a directional coupler. A circulator provides isolation between the transmitted and the back-scattered signal. The I-Q mixer combines the reference signal with the received signal to obtain the phase information from the base-band signal. The in-phase component, $I(t) \propto cos[\varphi(t)]$, and the quadrature component, $Q(t) \propto sin[\varphi(t)]$, of the mixer are used to determine the phase information in (1) as

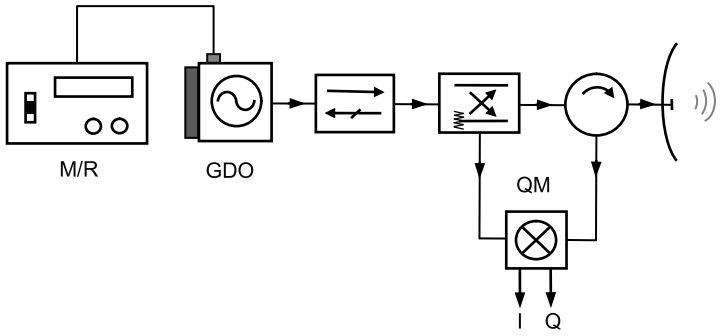

Fig 1. Schematic diagram of the MMW sensor front-end consisting of the modulator/regulator (M/R), Gunn diode oscillator (GDO), isolator, coupler, circulator, quadrature mixer (QM), and antenna.

$$\varphi(t) = \arctan\left[\frac{Q(t)}{I(t)}\right] \tag{3}$$

A 15.25 cm (6.0 in.) Gaussian optic lens antenna was used to focus the beam on the target. A corrugated horn served as the feed to the lens antenna. The specified gain of the antenna system was 43 dB, translating to a half-power beamwidth of approximately 1.2 degree at the operating wavelength of 3.2 mm. A scope was mounted over the lens for the purpose of beam alignment. All data acquisition and analysis was carried out by computer-based hardware and software using a four-channel, 24-bit data acquisition board. The commercially available software (LabVIEW™) was used for all acquisition and in-line processing operations.

IV. Experimental Observations

A series of experiments have been conducted to assess the capability of the MMW sensor to remotely measure human vital signs. Initial tests focused on validation of the MMW sensor response through comparison with data collected with a commercial optical vibrometer by using a simulated target. The results of those tests also served as the basis for assessing the sensitivity and detection limit of the MMW system. In the subsequent tests heart and respiration data were collected from a subject at different standoff distances. Based on the experimental observations, a series of routines were developed and adapted for extraction of biosignals of interest. The results of those investigations are described below.

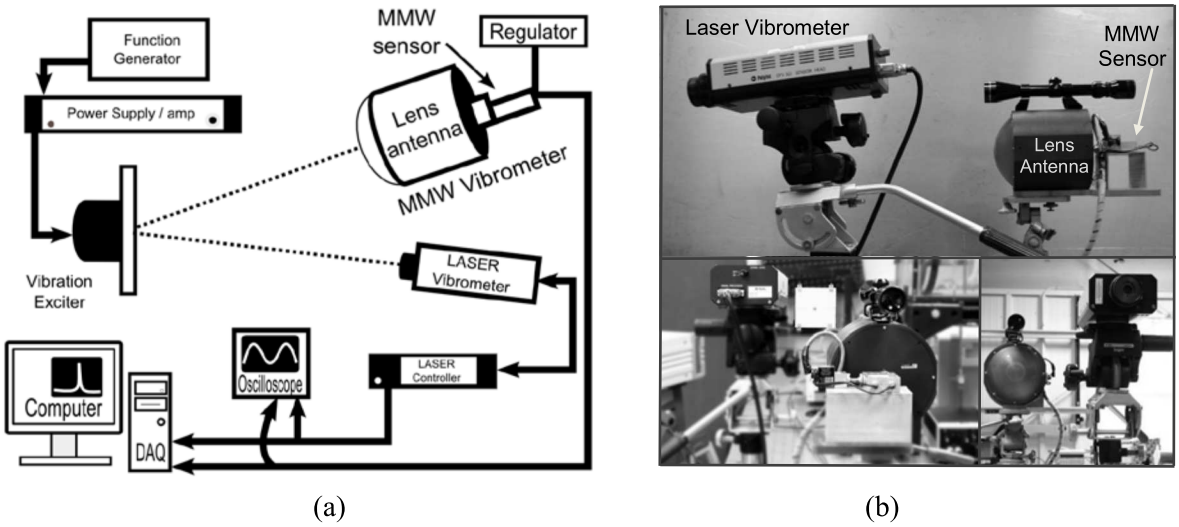

Fig 2. (a) Depiction of the apparatus used for evaluation of the MMW sensor for remote detection of vital signs. Also shown is (b) a picture of the laboratory setup showing (top) the laser vibrometer (left) and MMW sensor (right) and (bottom) the front and back view of the two systems along with the target (white square) shown in the bottom left picture.

A. Vibrometry Apparatus

In Fig. 2(a), the main components of the laboratory setup used to carry out the initial feasibility studies are shown [16]. A commercial optical vibrometer (633 nm wavelength class-II helium neon laser) with nanometer range out-of-plane displacement resolution was used for verification purposes by placing an optical reflector on the target. For the initial validation tests, data was simultaneously collected with the laser vibrometer and the MMW sensor to determine the correlation between the two signals. Pictures of the MMW sensor and the laser vibrometer from different view angles are displayed in Fig. 2(b). A mock-up structure fitted with a vibration exciter was assembled to simulate multimode target displacements. An arbitrary function generator in conjunction with a power amplifier provided the input signal to the vibration exciter.

A LabVIEW^{TM} virtual instrument (VI) was implemented to allow multi-channel recording and real-time processing and visualization of the sensor output as one-dimensional time traces, frequency spectrum, and two-dimensional time-frequency image (spectrogram). A graphical user interface (GUI) was developed under the MATLAB^{TM} environment for post processing of recorded data. The GUI is implemented in a modular fashion and allows one to conveniently update the existing functions (filters) or create and interface new algorithms under the GUI independent of the core source code.

B. Verification Tests

A series of tests on remote detection of physiological movements were conducted first by using the simulated target setup shown in Fig. 2. Displacements associated with respiration and heartbeat were simulated by using the vibration system described above. Verification of the MMW sensor readings was made through comparative measurements using the laser vibrometer signal as the reference. Data in all cases was digitized at a rate of 1 kHz and down-sampled later, typically by a factor of 1/8, for subsequent analyses through a software-based resampling of data. The surface of the target (solid block) was covered with a 10 mm thick layer of lossy dielectric material (rubber sheet) to somewhat represent reflection from human body. The arbitrary function generator was used to construct an ideal vital signal composed of a tapered-edge pulse and a *Sinc* function, $Sin(x)/x$, that represented chest movements associated with the respiration and cardiac function, respectively, which was amplified and fed to the vibration exciter. The respiration rate (RR) in this case was set to 0.36 Hz and the heart rate (HR) was set to 1.1 Hz. The selected heartbeat and respiratory frequencies are within the normal range of values reported in the literature. Significant variability, however, exists among the reported values in the open literature for the level of chest wall motion associated with cardiac activity measured using contact and non-contact sensors. The scatter in displacement values is in part due to such factors as age, health, weight and physiological differences among individuals in general. Depending on the location over the chest area where the measurement was performed and the position of the test subjects (standing, sitting, or lying on

the back) the values range from slightly less than 0.04 mm to greater than 1 mm. With an optical reflector placed on the mockup target, the laser vibrometer readings, used as reference in our experiment, indicated a maximum displacement of ~0.04 mm for the respiration function and roughly a third of that for the heart function. It is worth noting that the simulated level of displacement here is well below the minimum level of reported chest movement due to the cardiac and the respiratory function.

Figure 3(a) and (b) display 8 s tracings of the laser vibrometer and the MMW sensor data collected at a standoff distance of ~5 m, which closely resemble the output of the function generator. Both the RR and the HR waveforms are clearly discernible in those traces. The frequency spectrum of the time domain MMW data is shown in Fig. 3(c) for the 0.5 Hz to 20 Hz frequency range. With the fundamental RR component at 0.36 Hz having been intentionally cut out, the first harmonic of RR at 0.73 Hz and the fundamental frequency of HR at 1.1 Hz are the dominant components in Fig. 3(c). All the higher order

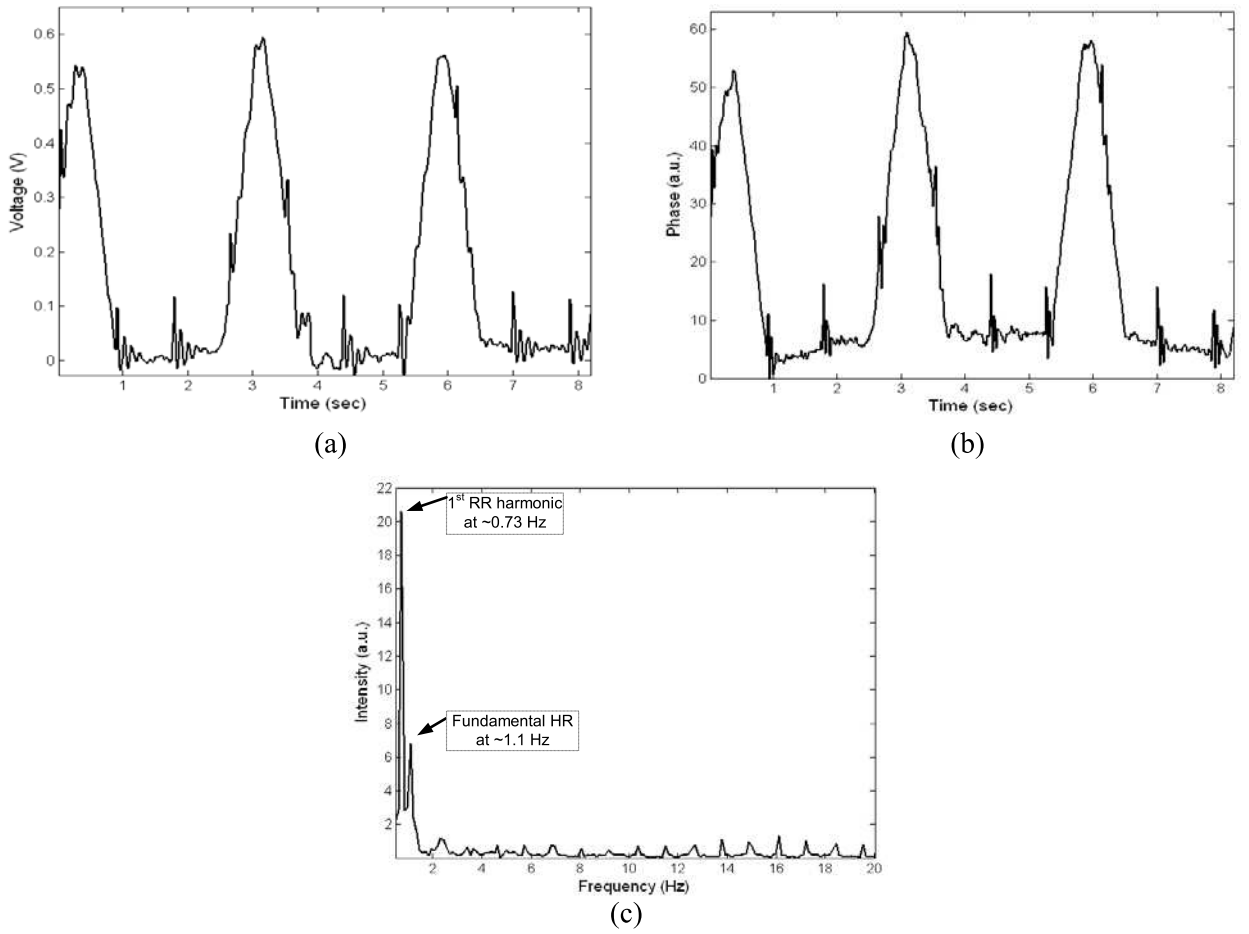

Fig 3. Comparison of recorded data over an 8 s interval with (a) laser vibrometer and (b) MMW sensor at a distance of ~5 m with the simulated biosignal composed of ~0.36 Hz respiration rate and ~1.1 Hz heart rate component. Also shown is (c) the MMW signal frequency spectrum for frequencies between 0.5 Hz and 5 Hz for an 8 s interval, with the first harmonic of RR and the fundamental HR component marked on the plot.

harmonics of the simulated HR with 1.1 Hz frequency separation are also visible in that figure. The results of this experiment and a number of similar comparative tests at different ranges clearly demonstrated the validity of the MMW sensor recordings.

C. Extraction of Vital Sign Signals

Physiological movements less than $\lambda/2$, where λ is the operating wavelength, may be measured without ambiguity with the MMW interferometer system described above. In reference to (1), this is done by converting the I-Q mixer outputs, representing the real and imaginary parts of a complex signal, directly to displacement values. Phase angle ambiguities, however, will be encountered when the displacement of the target is greater than $\lambda/2$. Furthermore, presence of stationary and systematic reflections from the target and nearby objects are common sources of interference that can further complicate extraction of signals of interest associated with vital signs from the composite sensor data. To alleviate this problem, signal processing algorithms employing mean centering and phase unwrapping of data were implemented. A flowchart describing different stages of signal processing applied to the MMW sensor data is provided in Fig. 4. Mean centering was done by subtracting the geometric mean vector of the complex output trace from each recorded data point. The baseline nulling process helps both to suppress any offset between the two channels and to eliminate the offset introduced by other sources of interference, thus allowing for determination of the true phase by shifting the I-Q signal trajectory to the

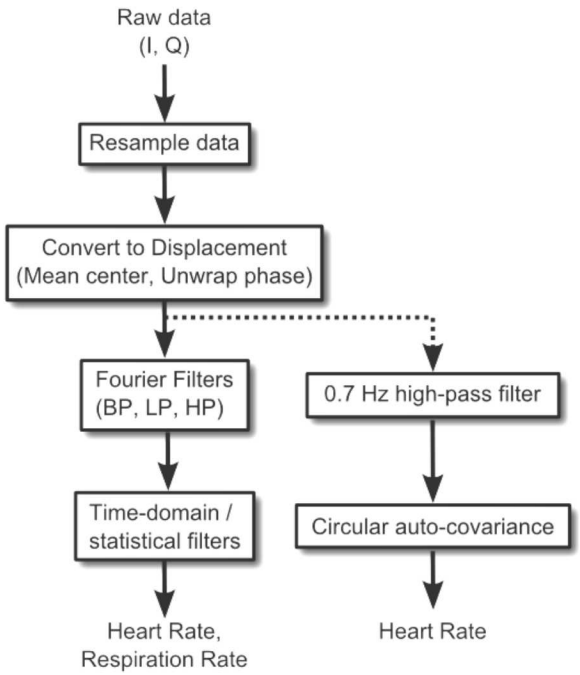

Fig 4. A flowchart describing common stages of signal processing applied to the MMW sensor output for extraction of vital sign data.

center of the complex plane. A phase unwrapping algorithm was subsequently applied to the mean-centered data in order to generate an unambiguous phase trace. The phase unwrapping routine essentially adjusts phase discontinuities greater than $\lambda/4$ to their $\lambda/2$ complement, which in turn is converted to displacement values in accordance with (1).

To demonstrate the validity of the algorithms described above, a series of experiments simulating multiple-wavelength displacements of the target were conducted. In the representative case discussed next, the vibration exciter was fed with a composite signal consisting of a 1 Hz HR, a 0.5 Hz RR, and a slow varying (~0.1 Hz) background fluctuation. The real and imaginary components (I and Q channels) of the raw data collected with the MMW sensor over an 8 s interval is shown in Fig. 5(a). The frequency spectrum of the complex signal is shown in Fig. 5(b). The displacement trace for the same data segment and the associated frequency spectrum following the application of the mean-centering and phase unwrapping algorithm is shown in Fig. 5(c) and 5(d), respectively. While the trace in Fig. 5(c) is a

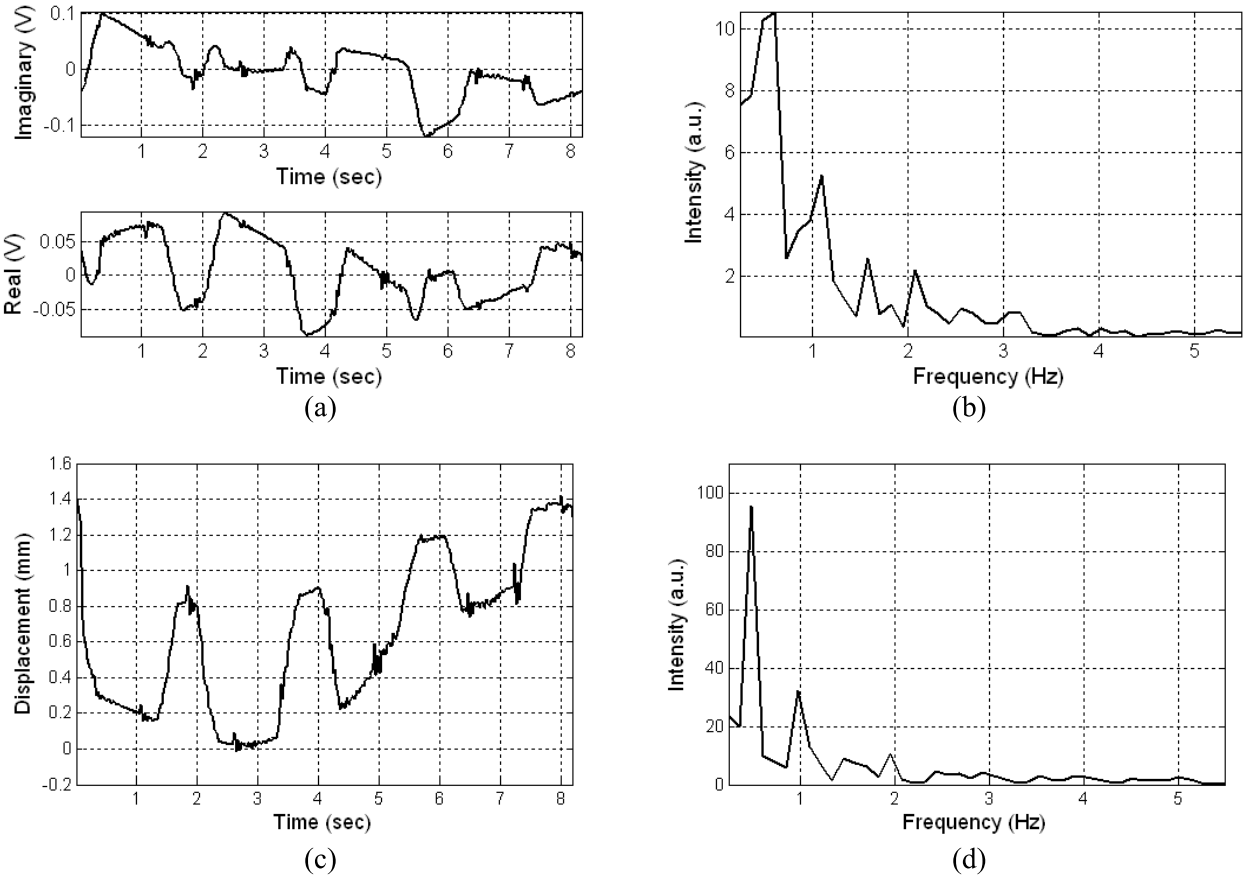

Fig 5. Estimation of RR and HR from the MMW sensor data collected using a simulated target excited simultaneously with a 1Hz heart-beat, 0.5 Hz breathing, and a 0.1 Hz sinusoid background movement. Shown here are (a) raw signal components over an 8 s interval and (b) associated frequency spectrum suggesting inaccurate estimation of HR and RR, and (c) processed data converted to displacement trace and (d) its frequency spectrum with the HR and RR fundamentals corresponding precisely to the actual frequencies set by the function generator.

physically pertinent representation of the true displacement of the target, neither of the raw amplitude tracings in Fig. 5(a) tracks the entire range of target movement. Furthermore, while phase ambiguities introduced by target displacements greater than $\lambda/2$ result in inaccurate estimates of RR and HR frequency in Fig. 5(b), the frequency spectrum of the processed trace shown in Fig. 5(d) correspond precisely to the actual RR and HR frequencies set by the function generator.

Although the signal processing steps described above provide a reliable means for conversion of I-Q sensor output to displacement values, arbitrary removal of mean baseline vector could lead to erroneous estimation of phase angle when the displacement of the target is less than $\lambda/2$ over the measured time interval. Correct estimation of the offset vector is particularly important when I and Q channels are not perfectly balanced (e.g., presence of a DC offset in mixer output) or a systematic drift is present. This problem may be alleviated by either using previously stored data or through periodic calibrations, which may simply be performed by artificially introducing multiple wavelength displacements. Representative displacement data collected with the MMW sensor from a subject over a relatively long time interval is shown in Fig. 6. The data was collected from at a distance of approximately 5 m with the antenna pointed at the subject's chest. Roughly one third of the data, composed of 43 segments, represents the period of inactivity (i.e., subject not being monitored) in the middle portion of the trace. The displacement data in

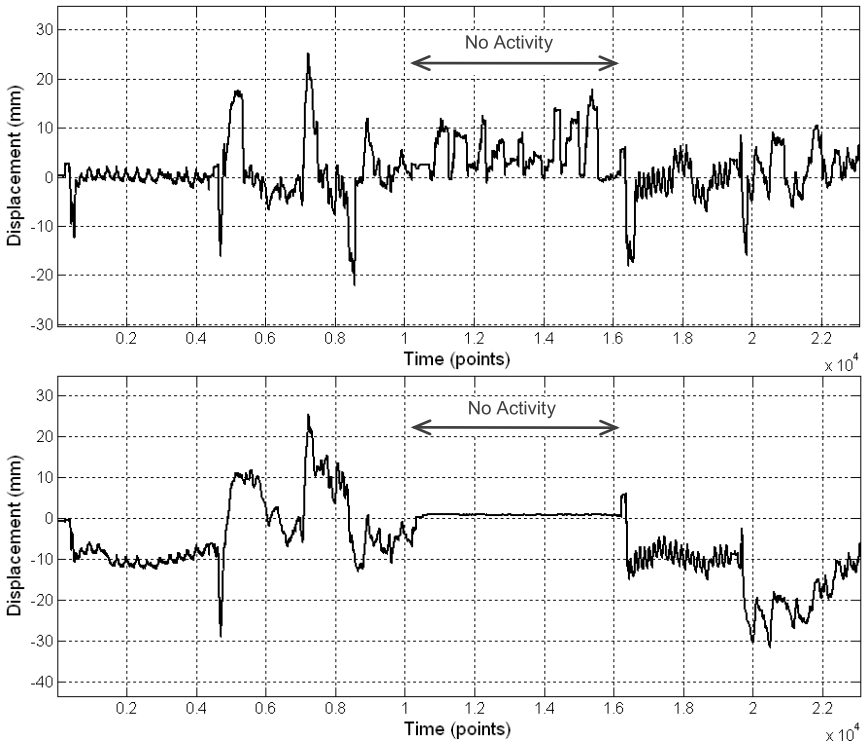

Fig 6. MMW sensor recording composed of 43 data segments combined and converted to displacement. The phase unwrapping was performed (top) independently for each segment and (bottom) unwrapped using all the recorded segments after interpolating between consecutive segments.

Fig. 6(a) was calculated by removing the offset and unwrapping the phase information independently for each short data segment. The trace in Fig. 6(b) on the other hand was calculated by first interpolating between consecutive data segments and subsequently removing the offset and unwrapping the phase using all the previously stored data points. Comparison of the two traces in Figs. 6(a) and (b) shows only the latter trace displaying correct unwrapping of phase information during the inactive portion.

Selected segments from the long trace shown in Fig. 6 are next used to further demonstrate the ability of the MMW sensor to remotely monitor physiological movements at relatively long standoff distances. Raw and processed data representing an 8 s recording of heart and respiration functions from a subject after a brief period of light physical activity are shown in Fig. 7. The data was collected while the subject was stationary. The original I- and Q-channel signals, the frequency spectrum of the 8 s recording as well as the time-frequency image of the entire data, which displays over 8 minutes of recording, are shown in Fig. 7(a). The associated processed data is shown in Fig. 7(b). While no clear features are discernible from either the time trace or the frequency spectrum of Fig. 7(a), both heartbeat and respiration signals as well as the associated frequency components can be clearly observed in Fig. 7(b). The estimated value of HR in Fig. 7(b) is around 95 beats per minute (bpm).

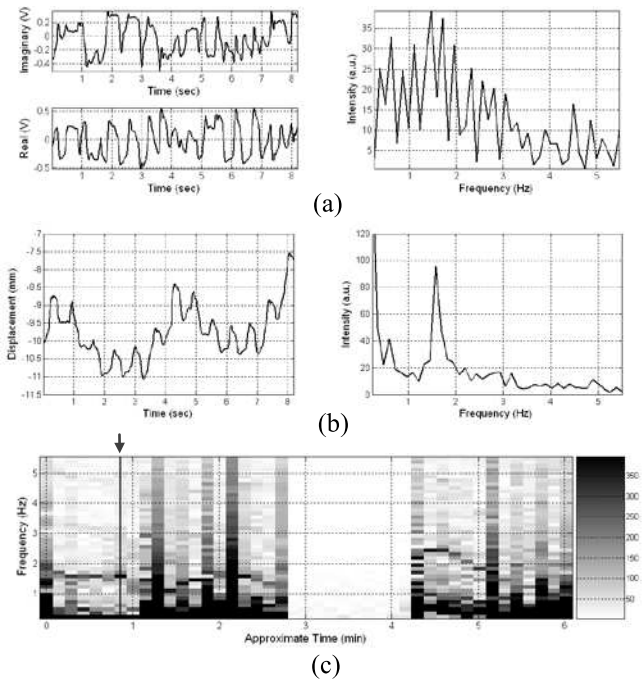

Fig 7. Measurement of vital signs from a standoff distance of approximately 5 m showing an 8 s trace of (a) raw signal components and their frequency spectrum, (b) displacement trace and its frequency spectrum, and (c) time-frequency image display of the displacement data covering 6 minutes of recording with an arrow marking the cross-section shown in (a) and (b).

As demonstrated above, extraction of vital sign signals from the MMW sensor data may be performed effectively when the target is stationary. Detection of faint signals associated with subtle physiological movements is an inherently challenging problem for non-stationary subjects. In those cases, it becomes necessary to track the target during the monitoring interval. No automatic tracking capability has yet been integrated into the MMW system described here. Therefore, to maintain the beam spot (~10 cm at a target distance of 5 m) over roughly the same region on the target, lateral movement was limited to less than half the spot size in either direction. A series of conventional frequency and time domain filters have so far been implemented to primarily help improve signal-to-noise ratio (S/N) through selective suppression of unwanted signals from the composite sensor recording. The primary feature of the Fourier domain filters is their sharp cut-off frequencies allowing isolation of low-frequency vital sign signals in presence of a wide range of interfering signals. Statistical filters have also been used to effectively extract heart and respiration rate.

Although not described in this article, as part of the on-going investigations, various signal enhancement methods including matched filtering, least-squares-based fitting, and statistical filtering algorithms are currently being developed to allow more efficient extraction of faint biosignals in presence of excessive background interference. One such filter used for discrimination of heartbeat and respiration rate in our study is the covariance filter. The auto-covariance function provides a measure of harmonic covariance in a time series, thus allowing enhancement of quasi-periodic features. The circular cross-covariance of vectors A and B may be written as

$$C(k) = \frac{\sum_{n} \left[A(n) - \overline{A}\right] \times \left[B(n+k) - \overline{B}\right]^{*}}{\left\|A - \overline{A}\right\| \times \left\|B - \overline{B}\right\|} \tag{4}$$

where B is shifted circularly by k samples. In the case of auto-covariance, B is a shifted version of A.

Representative test cases on the use of circular auto-covariance for extraction of HR in presence of background interference associated with target motion is demonstrated next. This particular filter was employed both because of its ability to effectively isolate weak HR signals at larger standoff distances and because of the computational efficiency of the algorithm for real-time processing of the data. Two separate segments from the remotely monitored MMW recording shown previously in Fig. 7 were used for this purpose. The first segment was collected with the subject at rest following a brief period of light physical activity and the second segment was collected by monitoring the subject after a short period of more intense physical activity. Processed data for both cases are shown in Fig. 8. The measured displacement data with the MMW sensor were processed by first applying a 0.7 Hz high-pass Butterworth filter of fifth order to remove the respiratory signal as well as any low-frequency baseline followed by the circular auto-covariance filter, which was applied in a piecewise manner to enhance the heartbeat signal.

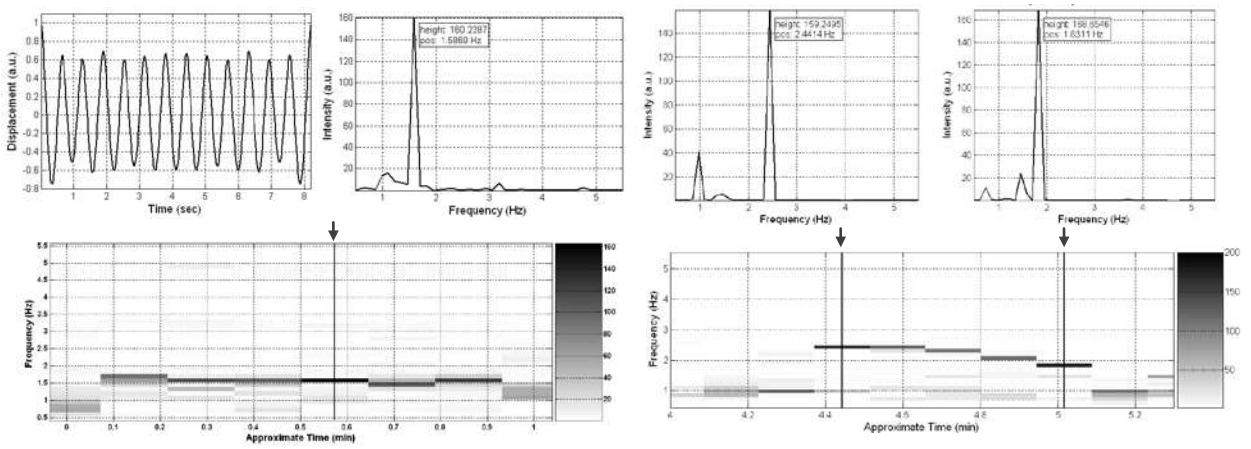

(a) (b)

Fig 8. Selected data segments from Fig. 7 for the case of subject at rest after a brief period (a) of light and (b) more intense physical activity. The time-frequency image display of data over the roughly 1 minute monitoring intervals is shown. Arrows mark the location of time frames for which the displacement trace and frequency spectrums are displayed in each plot.

The data associated with the subject being monitored remotely after a brief period of light activity is shown in Fig. 8(a). The dominant band in the time-frequency image display exhibits a nearly constant frequency of 1.58 Hz, translating to a HR value of 95 bpm, over an approximately 1 minute monitoring interval. The filtered displacement trace for an 8 s time frame and the associated frequency spectrum are also shown in that figure. The data segment associated with monitoring of the subject after a brief period of more intense physical activity is shown in Fig. 8(b). The frequency spectrum for two 8 s time frames that are roughly 30 s apart are also shown in that figure. Based on the dominant frequency component, the estimated value of HR for the time frames at approximately 4.5 minutes and 5 minutes show elevated HR of 146 bpm and 110 bpm, respectively. The dominant band in the time-frequency image display of Fig. 8(b) exhibits a downward trend toward the mean value of HR in Fig. 8(a) when the subject was at rest. The results here clearly demonstrate the ability of the MMW sensor to monitor changes in vital signs over an extended period of time.

Finally, representative test cases are shown to qualitatively demonstrate the effect of range on remote monitoring of vital signs with the MMW sensor described in this article. Data collected from a subject at rest from a distance of approximately 3.5 m is shown in Fig. 9. The raw signal was processed in the same manner as that described for the previous two examples. The time-frequency image display of the processed data in this case shows a flat dominant band around 1.1 Hz over the entire 2.5 minute recording interval. The dominant frequency component associated with a HR value of around 66 bpm is clearly detectable in all 8 s frames. The MMW sensor recording from a subject at a distance of 15 m is shown in Fig. 10. In this case the subject was monitored immediately after a brief period of light activity.

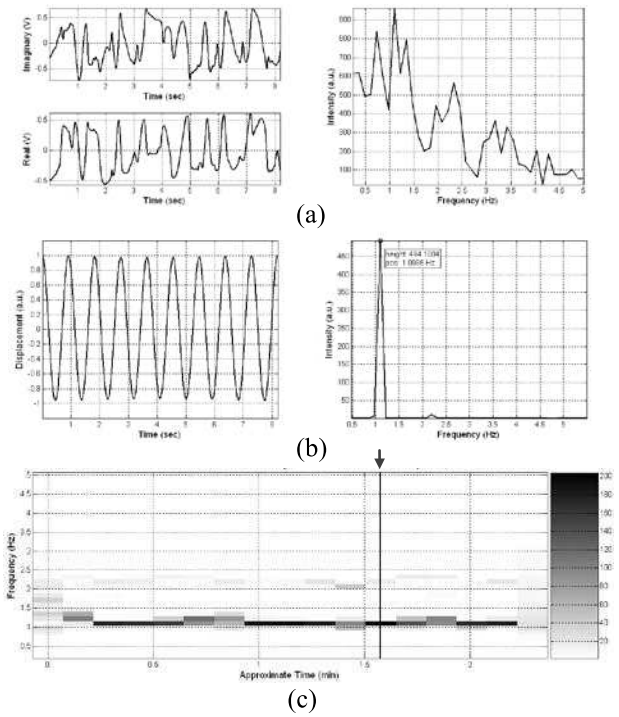

Fig 9. MMW sensor data collected from a subject at rest from a distance of approximately 3.5 m showing (a) raw data from I and Q channels, (b) filtered displacement data and its frequency spectrum for a selected 8 s frame, and (c) time-frequency image display of data for roughly a 2.5 minute monitoring interval.

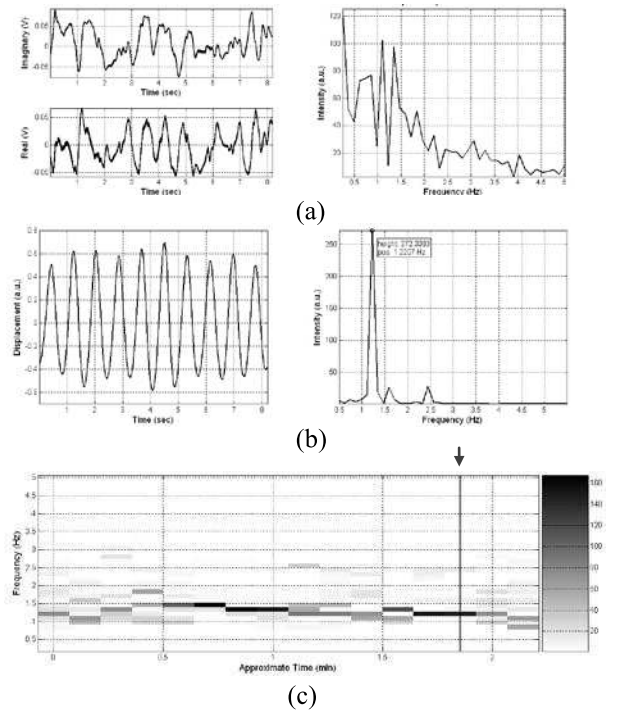

Fig 10. MMW sensor data collected from a subject at rest from a distance of approximately 15 m showing (a) raw data from I and Q channels, (b) filtered displacement data and its frequency spectrum for a selected 8 s frame, and (c) time-frequency image display of data for roughly a 2 minute monitoring interval.

Although the increase in distance resulted in some loss in S/N, the HR value is clearly detectable in majority of time frames over the roughly 2 minute monitoring interval. Furthermore, at this distance, the strength of the signal associated with heartbeat is sufficiently high to monitor the change in HR, from an elevated value of approximately 90 bpm to a rest value of approximately 70 bpm, over the monitoring interval. The results of investigations on assessing the detection limit of the MMW system using a mock-up structure have been reported elsewhere [16]. Those studies demonstrated the ability of the system to clearly resolve (S/N > 2) a 20 μm displacement at a distance of 50 m (~150 ft.). While systematic studies are currently under way to quantitatively determine the upper limit of detection range for reliable monitoring of human vital signs, the results of investigations performed so far suggest that the detection range for the low-power MMW sensor described in this article is expected to be higher than 15 m. This range is significantly higher than that commonly reported using microwave devices for monitoring human vital signs.

V. CONCLUSION

A 94 GHz compact MMW sensor for remote monitoring of human vital signs has been developed and its functionality has been demonstrated. The sensor provides higher directivity, increased sensitivity, and longer detection range in comparison to its microwave counterparts. The MMW front-end employs all solid-state active and passive block-type components and can be battery operated. A number of signal processing and data analysis algorithms have been developed or adapted for effective extraction of typically faint signals associated with physiological movements in presence of strong stationary and systematic reflections. Based on the measured S/N values from laboratory experiments performed to date at standoff distances of up to 15 m, the upper limit of the detection range is expected to be greater than 15 m. On-going investigations are currently focused on implementation of improved signal processing and data analysis algorithms for extraction of vital sign signals under difficult test conditions. To further reduce the size of the MMW sensor, the use of compact high-gain Gaussian optic antenna designs such as dielectric-loaded horn antennas are also being evaluated. An automatic target tracking system is also under development. It is envisaged that the MMW system described in this article may be adapted for use in a wide range of standoff sensing applications including for patient health care, structural health monitoring, nondestructive testing, biometric sensing, and remote vibrometry in general.

ACKNOWLEDGEMENT

This work was supported in part by the U.S. Department of Energy under Contract DE-AC02-06CH11357 and in part by the National Consortium for Measurement and Signature Intelligence (MASINT).

REFERENCES

[1] K.M. Chen, D. Misra, H. Wang, H.R. Chuang, and E. Postow, "An X-band microwave life-detection system," IEEE Trans. Biomed. Eng., vol. 33, pp. 697–702, July 1986.

[2] J. C. Lin, "Microwave Sensing of Physiological Movement and Volume Change: A Review," Bioelectromagnetics 13:557-565 (1992).

[3] K.M. Chen, Y. Huang, J. Zhang, and A. Norman, "Microwave life-detection systems for searching human subjects under earthquake rubble and behind barrier," IEEE Trans. Biomed. Eng., vol. 27, pp. 105–114, Jan. 2000.

[4] J. Geisheimer and E.F. Greneker, "A Non-Contact Lie Detector using Radar Vital Signs Monitor (RVSM) Technology," IEEE AESS Systems Magazine, pp. 10-14, Aug. 2001.

[5] O. Boric-Lubecke, P.W. Ong, and V. Lubecke, "10 GHz Doppler radar sensing of respiration and heart movement," Proc. of IEEE 28th Annu. Northeast Bioengineering Conf., pp. 55–56, Apr. 2002.

[6] A.D. Droitcour, O. Boric-Lubecke, V.M. Lubecke, J. Lin, and G.T.A. Kovac, "Range correlation and I/Q performance benefits in single-chip silicon Doppler radars for noncontact cardiopulmonary monitoring," IEEE Trans. Microwave Theory Tech., vol. 52, pp. 838–848, Mar. 2004.

[7] C. Li, Y. Xiao, and J. Lin, "Experiment and Spectral Analysis of a Low-Power Ka-Band Heartbeat Detector Measuring From Four Sides of a Human Body," IEEE Trans. Microwave Theo. Tech., Vol. 54, No. 12, pp. 4464-4471, Dec. 2006.

[8] C. Li Changzhi and J. Lin, "Optimal Carrier Frequency of Non-contact Vital Sign Detectors," Proc. Of IEEE Radio and Wireless Symposium, 2007, pp. 281–284, 2007.

[9] C. Li and J. Lin, "Random body movement cancellation in Doppler radar vital sign detection," IEEE Trans. Microwave Theory Tech., vol. 56, no. 12, pp. 3143–3152, Dec. 2008.

[10] M. Pieraccini, G. Luzi, D. Dei, L. Pieri, and C. Atzeni, "Detection of Breathing and Heartbeat Through Snow Using a Microwave Transceiver," IEEE Geoscience and Remote Sensing Letters, vol. 5, NO. 1, Jan. 2008.

[11] D. T. Petkie, C. Benton, and E. Bryan, "Millimeter wave radar for remote measurement of vital signs," Proceedings of the IEEE Radar Conference, pp. 1-3, 2009.

[12] D. T. Petkie, E. Bryan, C. Benton, C. Phelps, J. Yoakum, M. Rogers, A. Reed, "Remote respiration and heart rate monitoring with millimeter wave/terahertz radars," Proceedings of the SPIE, Vol 7117, 2008.

[13] N. Gopalsami, S. Bakhtiari, A. C. Raptis, S. L. Dieckman, and F. C. De Lucia, "Millimeter Wave Measurements of Molecular Spectra with Application to Environmental Monitoring," IEEE Trans. Instr. Meas., vol. 45, pp. 225-230,1996.

[14] N. Gopalsami and A. C. Raptis, "Millimeter-Wave Radar Sensing of Airborne Chemicals," IEEE Trans. Microwave Theory Techniques, vol. 49, pp. 646-653, 2001.

[15] N. Gopalsami, S. Bakhtiari, T. W. Elmer, and A. C. Raptis, "Application of Millimeter-Wave Radiometry for Remote Chemical Detection," IEEE Trans. Microwave Theo. Tech., Vol. 56, No. 3, pp. 700-709, Mar. 2008.

[16] S. Bakhtiari, N. Gopalsami, T.W. Elmer, and A.C. Raptis, "Millimeter Wave Sensor for Far-Field Standoff Vibrometry," Review of Progress in Quantitative Nondestructive Evaluation, American Institute of Physics (AIP), vol. 28, 2009.